

Manuscript Draft

Manuscript Number:

Title: Snow avalanche energy estimation from seismic signal analysis

Article Type: Special Issue:EGU Snow & Avalanches 2006

Keywords: Seismic record; Snow avalanche; Energy; Surface waves.

Corresponding Author: Mr Ignasi Vilajosana,

Corresponding Author's Institution: University of Barcelona

First Author: Ignasi Vilajosana

Order of Authors: Ignasi Vilajosana; Emma Suriñach, Dr.; Giorgi Khazaradze, Dr; Peter Gauer, Dr

Abstract: A method to obtain the evolution of the seismic energy transmitted into the ground by a down going avalanche is presented. Estimations of this energy could be useful for model validation, avalanche size classification and to give information on the avalanche evolution. The method was applied to two different type avalanches. The analysed data came from Ryggfonn (Norway) avalanche experimental site operated by the Norwegian Geotechnical Institute (NGI) and recorded by the University of Barcelona seismic instruments during the artificially released avalanches of 2004/02/28 and 2005/04/15. The energy determination needs a prior seismic characterization of the site and the knowledge of the avalanche front speed. In this paper a seismic characterization (surface waves phase velocity and amplitude attenuation factor) of the Ryggfonn site is presented. This characterization will serve for subsequent studies. The main source of seismic signals for the studied events corresponds to basal friction and ploughing at the avalanche front in changes of slope; the latter causing high seismic energy dissipation. A comparison of the evolution of the seismic energy dissipated with the energy generated by a simple sliding block model of constant mass was performed. The differences observed highlight the importance of the ploughing, basal friction and length of the avalanche in the generation of seismic energy. The total seismic energy dissipated for the two avalanches was obtained. Although they are classified of the same size, the seismic energy dissipated

reflects their different type. The dry/mixed event dissipates a smaller amount of energy (2.7 MJ) than the dry/dense event (4.2MJ).

Snow avalanche energy estimation from seismic signal analysis

I. Vilajosana¹, E. Suriñach¹, G. Khazaradze¹, P. Gauer²

¹*Grup d'Allaus (RISKNAT); Dept. de Geodinàmica i Geofísica, Universitat de Barcelona, Martí i Franquès s/n, 08028, Barcelona, Spain (vilajosana@ub.edu)*

²*Norwegian Geotechnical Institute, Postbox 3930 Ullevaal Stadion, N-0806, Oslo, Norway.*

Abstract

A method to obtain the evolution of the seismic energy transmitted into the ground by a down going avalanche is presented. Estimations of this energy could be useful for model validation, avalanche size classification and to give information on the avalanche evolution. The method was applied to two different type avalanches. The analysed data came from Ryggfonn (Norway) avalanche experimental site operated by the Norwegian Geotechnical Institute (NGI) and recorded by the University of Barcelona seismic instruments during the artificially released avalanches of 2004/02/28 and 2005/04/15. The energy determination needs a prior seismic characterization of the site and the knowledge of the avalanche front speed. In this paper a seismic characterization (surface waves phase velocity and amplitude attenuation factor) of the Ryggfonn site is presented. This characterization will serve for subsequent studies. The main source of seismic signals for the studied events corresponds to basal friction and ploughing at the avalanche front in changes of slope; the latter causing high seismic energy dissipation. A comparison of the evolution of the seismic energy dissipated with the energy generated by a simple sliding block model of constant mass was performed. The differences observed highlight the importance of the ploughing, basal friction and length of the avalanche in the generation of seismic energy. The total seismic energy dissipated for the two avalanches was obtained. Although they are classified of the same size, the seismic energy dissipated reflects their different type. The dry/mixed event dissipates a smaller amount of energy (2.7 MJ) than the dry/dense event (4.2MJ).

Email address: vilajosana@ub.edu, FAX:+34-93-402-13-40

Keywords: Seismic record, Snow avalanche; Energy; Surface waves.

1. Introduction

Estimations of the seismic energy transmitted into the ground by snow avalanches could be useful for model validation and avalanche size classification. Moreover, evolution of the energy transmitted into the ground could give information on the source of the seismic signals generated by an avalanche and, in consequence, on the evolution of the avalanche. In addition, similar to earthquakes, the estimation of the radiated energy by snow avalanches can provide good estimates of their magnitude which could be used as a new tool to classify avalanches. Unlike other physical parameters (impact pressure, snow deposit density), there are few estimations on the energy dissipated by snow avalanches. In this paper a method to estimate the energy transmitted into the ground by snow avalanches using seismic observations is presented.

In general, it is known that stronger ground vibrations are observed with denser avalanches. However, the exact nature of energy conversion from potential to seismic energy during the avalanche propagation is not known. In this paper we also aim to clarify this point.

A significant amount of the potential energy of a snow avalanche propagating down the slope is spent in overcoming the resistance of the flow at the fluid/solid interface. This energy is transformed into a combination of heat, ground vibration and sound waves.

The energy transmitted into the ground by snow avalanches, besides the impacts produced by intrinsic elements travelling inside the flow, is mainly attributed to the friction produced by the bottom of the avalanche in contact with the ground. Earlier studies carried out by Suriñach et al. (2000 and 2001) where video images and seismic signals from snow avalanches were compared, demonstrated that the most energetic peaks of the seismic signals coincided with the passing of the avalanche front through a change of slope. However, no quantification of the transmitted energy was given.

Firstov et al., (1990) presented one of the firsts studies on energy transmitted into the ground by snow avalanches using seismic data, however, the method used was not presented in detail. For other natural phenomena, such us Tornados (Tatom and Vitton, 2001) and debris flows (Suwa et al., 2003), similar techniques have been presented to obtain the energy transmitted into the ground and proved to be useful for the event magnitude classification.

In this paper the evolution of the energy transmitted into the ground by two avalanches was calculated using the method presented. We took advantage of the availability of two seismic stations installed in an avalanche experimental site, and that their spatial location was suited for the developed methodology. Additionally, the energy evolution estimates were compared with simple sliding block models (Kanamori, H., and J. W. Given., 1982, Brodsky et al., 2003) to asses the reliability of the methods.

The analysed data came from Ryggfonn (Norway) avalanche experimental site operated by the Norwegian Geotechnical Institute (NGI) (Lied et al., 2002) and recorded by the University of Barcelona seismic instruments during the artificially released avalanches of 2004/02/28 and 2005/04/15. In addition, these data were complemented with the speed evolution profiles for the analysed events, which were obtained from the analysis of video images recorded by NGI and PCM model numerical simulation (Perla et al., 1980).

The avalanche group at the Universitat de Barcelona (UB) has been studying the seismic signals generated by avalanches at different sites in Europe since 1994 (Suriñach, 2004). The recent studies of the group have focused on: the identification of the main sources of the seismic signals produced by snow avalanches, the determination of avalanche front speeds and the characterization of avalanche seismic signals for detection purposes. (e.g. Biescas et al., 2003; Suriñach et al., 2005; Vilajosana et al.,

2006). The method for the energy determination of avalanches presented here is a continuation of these previous studies.

2. Experimental Site and Data

The Ryggfonn full-scale avalanche site, situated 500 km north-west of Oslo, Norway, was set up to study snow avalanches by the NGI in 1980 (Lied et al., 2002). Since then, approx. 2-3 avalanches per year have been released at this site. The avalanche path at Ryggfonn has a vertical drop of 900 m and a horizontal length of 2100 m (Figure 1). The avalanches released at the site according to the Canadian snow avalanche size classification (McClung and Schaerer., 1993) range in size between 2 (mass of 100 T) and 4 (mass of 10.000 T), and occasionally may even reach class 5 (mass of 100.000 T). Their maximum velocities can reach 60 m/s. A retaining dam of unconsolidated material, 16 m in height and 75 m in crown length is installed in the lower part of the avalanche path. This dam is equipped with different instruments (Figure 1). In the period of 2003-2006 the University of Barcelona avalanche research group installed two 3D seismometer Lennartz 3D-5s. One of the sensors (UBtrack) was buried in the ground, 100 m up-slope of the dam in the avalanche path and the other one (UBhut) was situated at 410 m from the dam to the east down in the Valley (Figure 2). A 4.5 m high concrete structure containing three load cells is placed approx. 230 m up-slope from the dam also in the main avalanche path. Moreover, a 5.5 m high cylindrical steel tower equipped with two more load cells and one geophone (GF1) which triggers the recording system is placed 90 m above this structure (Figure 1). A shelter containing control and recording instruments is located in the valley 500 m east of the dam. The shelter is provided with power, telephone line and ISDN connection. The recording system consists of a data-logger REFTEK DAS 130-06, which is triggered by GF1

geophone when the avalanche front hits the steel tower. The data are recorded at a sampling rate of 200 sps. A GPS antenna installed on top of the shelter provided accurate base of time.

In this study we analyzed the seismic data recorded by University of Barcelona from the avalanches of 2004/02/28 and 2005/04/16. Henceforth referred as events A and B. Event A was an artificially released dry/mixed medium sized (Size 4) avalanche. A subsequent field survey showed that although much of the debris was retained by the dam, the dust cloud went far beyond. The volume of the deposit in the run-out zone below the load cells on the concrete structure was estimated to be around 100,000 m³. The speed estimates of the avalanche on the upper part of the path were provided by NGI from a numerical simulation of the flow using a PCM model (Perla et al., 1980).

Event B was an artificially triggered medium sized (Size 4) dry/dense avalanche with a frontal aerosol part which disappeared 100 m upslope of the dam. In the lower part of the path wet snow was incorporated into the avalanche. In order to obtain speed estimates of the avalanche on the upper part of the path, video images from the event were recorded. Useful data in the interpretation of the results from the subsequent field survey of the event included cartography of the deposits, snow depth and density of the snow in the deposition area (Gauer and Kristensen, 2005).

3. Data Analysis and Methodology

Our previous studies on avalanche wave characterization showed that the seismic signals generated by snow avalanches are mainly composed of surface waves (Suriñach et al., 2001). For this reason, the seismic energy transmitted into the ground by the avalanche is obtained following the methodology proposed by Suwa et al., (2003) which is suitable for surface waves. If we assume that the near surface ground is

homogeneous and isotropic (or that the local ground heterogeneities are smaller than the seismic signal wavelength considered, in our case from 70 m to 2777 m), the total amount of energy dissipated for surface waves over a cylindrical wave front (Figure 3) can be calculated as:

$$E_s = \int_{t_1}^{t_2} \int_{f_1}^{f_2} \rho \cdot c \cdot A(t)^2 \cdot 2\pi \cdot r(t) \cdot h \cdot e^{\frac{\pi \cdot f \cdot r(t)}{Q(f) \cdot c}} df dt \quad (\text{Eq.1})$$

Where **A** is the amplitude of the ground motion recorded at the observation point in (m/s), **c** is the phase velocity of the seismic surface waves, **ρ** is the ground density, **r** is the distance avalanche front-seismometer, **h** corresponds to ¼ of the wave length (surface waves amplitude at depth h has been reduced by a factor 1/e and hence the contribution of deeper waves is not significant (Aki and Richards (1980)), **f** is the frequency in Hz and **Q(f)** is the amplitude attenuation factor for seismic waves at Ryggfonn. In this expression, the amplitude decay with time is produced by the geometric spreading of the waves and the anelastic attenuation of the amplitude with distance.

According to Eq. 1 the determination of the energy transmitted into ground should be a straightforward task. However, for snow avalanches this is not the case. The specific seismic characteristics of the site must be previously determined and a characterization of the seismic records produced by the avalanche must be performed. The process to obtain the seismic energy dissipated into the ground by the avalanche is summarized below: Site: 1) Phase velocity calculation for seismic waves at Ryggfonn site; 2) Amplitude attenuation factor determination at Ryggfonn site. Avalanche: 3) Determination of the distance avalanche front-seismometer per unit of time; 4) Avalanche seismic signal characterization; And Energy estimation: 5) Calculation of the

seismic energy dissipated for each frequency and each component of the seismic signals; 6) Integration over all frequencies and; 7) Integration over horizontal components.

3.1. Phase velocity calculation for seismic waves at Ryggfonn site

Taking advantage of the availability of seismic data from the explosions that triggered the artificially released avalanches (A, B) the determination of the phase velocities of the P, S and surface waves at this site was performed. The velocity of the P waves was obtained through the difference in the arrival time, performed by picking of the P wave generated by the explosion, at the two distinct seismometers (UBtrack and UBhut in Figure 2). The difference in the distance explosion-UBtrack in front of the distance explosion-UBhut, which is 181.44 m permitted this calculation. According to Aki and Richards (1980), S wave velocities are, in general, $V_s = \sqrt{3} \cdot V_p$ and the surface wave velocity, assuming a half space medium and accomplishing Poisson condition, is approximately $0.92V_s$. Combining this relationship with the assumption of planar waves, yields a phase velocity for superficial waves at Ryggfonn site of 2777 ± 175 m/s. Unluckily, only two explosions were available to perform this calculation; more data could have given more reliable results. However, the obtained values for the seismic wave propagation velocities seem to be reasonable estimates for the existing soil characteristics.

3.2. Amplitude attenuation factor determination at Ryggfonn site

To obtain an estimation of the amplitude attenuation factor Q for superficial waves at Ryggfonn, we adapted the methodology proposed by Jolly et al., (2002). We used the known locations of the explosions and the two seismic stations (Figure 2).

Basically, the method consists of determining the Q value that minimizes the difference in the amplitudes recorded at the two different seismometers corresponding to a same source, once they have been corrected by geometrical spreading and anelastic attenuation of waves due to the different distance explosion-seismometer. This process is performed in the time-frequency domain for convenience and each of the explosions signals is treated independently. The attenuation factor Q was estimated given that the location of the explosions that triggered the avalanches was known. To this end, 1) we selected in the time series (UBtrack and UBhut) the signals generated by the explosion that triggered the avalanche (A and B independently), 2) we calculated the Running Spectrum (RS) based on the Fast Fourier Transform (FFT) of the explosion signals recorded in UBtrack and UBhut. Subsequently, for each station the wave amplitude corresponding to the different frequency windows in the RS, $A(f)_i$, were obtained. The window frequency width was 0.8 Hz and the time resolution was 1.28 s, according to the data sampling rate and the resolution used to calculate the FFT. 3) The amplitude windows $A(f)_i$ were corrected for anelastic attenuation and geometrical spreading at several trial Q values (ranging from 1 to 100) using the following expression:

$$A_0(f) = A(f) \cdot \sqrt{\frac{r \cdot c}{f}} \cdot e^{\frac{\pi \cdot f \cdot r}{Q \cdot c}} \quad (\text{Eq. 2}),$$

Where the phase velocity c was obtained as described in section 3.1 and the explosion-seismometer distance r , was found from the Digital Terrain Model (DTM) provided by NGI. Consequently, we obtained the amplitude corrected values ($A_0(f, Q)_i$) for each frequency (f) and attenuation factor (Q) at each station (i), 4) for each frequency (f) the root mean square (RMS) logarithmic residuals of the corrected amplitudes ($A_0(f, Q)_i$) between the two seismometers was calculated (daRMS), 5) for each frequency f , the Q

value minimizing the RMS residual amplitude (daRMS), was also selected. This value corresponds to the Q value that best fits in the two independent stations. The same procedure was repeated for each of the available explosions, finally, 6) a linear relationship between the Q values in function of the frequency was obtained (Figure 4). The specific relationship for the Ryggfonn site can be given as: $Q = 0.087 \cdot f + 5.3$.

3.3. Distance avalanche front-seismometer

The avalanche front-seismometer distance (r), which varies in time, is necessary to determine the decay due to distance observed in the recorded seismic amplitudes (Eq. 1) (Figure 3). The speed of the avalanche front along the main propagation path is used to determine the location of the avalanche as function of time with respect to the location of the fixed seismometer. The arrival time of the P waves of the explosion at the sensor situated in the track (UBtrack) is fixed as the origin of time in the seismic time series. This time is attributed to be the beginning of the avalanche. The arrival time of the avalanche front over the sensor is determined using the RS as presented in Vilajosana et al., (2006). The time series corresponding to events A and B are shown in Figure 5. Avalanche speed values provided by NGI obtained from numerical simulations using PCM model (Perla et al., 1980) (Event A and B) and from video images (Event B) at several locations along the avalanche path were used to obtain the avalanche front-seismometer distance r (Figure 6). A PCM model with $\mu=0.22$ and $M/D=300$ was used for event A. These coefficients seemed to be reasonable according to the type and size of the event. However, independent speed measurements from load cells and geophones (Vilajosana et al., 2006) in the lower part of the path show higher speed values. Unfortunately, although the limitations of the PCM model, these are the only data

available for this event, since no direct speed measurements in the upper part of the path are available to assess the quality of the model estimation.

For event B, the avalanche front speed evolution at several locations along the main path was obtained using video images (Figure 6 right, dashed line). In addition, several PCM model simulations using distinct coefficients were carried out to complete this information. The parameters that best fitted the avalanche velocity evolution obtained using video images were $\mu=0.4$ and $M/D=500$ (Figure 6 right, continuous line). These values are in accordance with the type of flux observed during the event B.

3.4. Avalanche seismic signal characterization and processing

Before proceeding with the energy estimation, the time-frequency avalanche seismic signal characterization was necessary. The specific characteristics of the signals recorded during the events were determined in order to isolate the signals generated by the avalanche itself from the signals generated by other seismogenic sources. Each time series was filtered with a 1-40 Hz 8th order band pass Butterworth filter to obtain the band where the maximum seismic energy was concentrated in accordance with the information obtained in the total spectrum of the time signal. Moreover, a 17-21 Hz 4th order band reject filter was applied to remove the noise generated by the helicopter that was flying during the experiments (Biescas, 2003). Finally, for each component (N-S, E-W, Z), 17 “mono-frequency” time series were obtained by filtering the pre-filtered time series with overlapped windows 2 Hz wide, from the 1-3 Hz window to 37-39 Hz. The central frequency value of each window was considered to be the frequency of the “mono-frequency” filtered time series.

Earlier studies of our group in other sites, showed that main parts of the seismic signals generated by snow avalanches were composed of surface waves (Suriñach et al., 2001).

In consequence, we assume the same behaviour for the signals obtained at Ryggfonn. However, due to the importance of this assumption in the energy estimation, a ground particle motion analysis of the filtered signals obtained at Ryggfonn was performed to confirm this hypothesis (Figure 7).

In general, the vertical component, Z , of the seismic signal presents lower amplitude than the horizontal components (E-W, N-S). In addition, it is also observed that the ground particle motion for a number of wave packets is completely confined in the horizontal plane (this is specific for Love waves). The ground particle motion in other cases consists of elliptical motion in the vertical plane parallel to the direction of propagation of the avalanche (Figure 7). For these reasons we conclude that the main part of the seismic signals produced by the avalanches in Ryggfonn are superficial waves. In order to compare the energy estimations obtained using the seismic data recorded in UBtrack and UBhut, and to detect local site effects, the method of Nakamura (1989) was applied. The results showed that the energy estimations obtained in UBtrack and UBhut are of the same order.

3.5. Energy estimation

The energy dissipated by the surface waves was obtained following Eq. 1. For this purpose we only consider horizontal seismic components of the ground motion, assuming that the signals recorded in the vertical component are mainly produced by body waves. The seismic energy dissipated in each frequency in every seismic component of the ground motion was calculated using the corresponding “mono-frequency” seismic time series previously obtained (Sect. 3.4). The estimation of the energy dissipated in each seismic component was obtained from the summation of the different “mono-frequency” energy contributions. An estimation of the energy

corresponding to the horizontal components dissipated by the surface waves was obtained from the contributions of the N-S and E-W components. Figures 8 and 9 show the energy dissipated by these avalanches running down the main propagation path in function of the horizontal distance from the release zone.

4. Results and Discussion

Using the method described in the previous section we estimated the energy dissipated by surface waves for avalanches A and B. The estimates of the energy of the horizontal component of the seismic signals are presented in Figures 8 and 9. The energy estimations are presented as a function of the horizontal distance from the release zone. Note that a conversion time to distance was previously performed via section 3.3. The path profile is also indicated in these figures to help in the interpretation of the plot. The energy dissipated per unit of mass by surface waves using a simple sliding block model (see appendix) is also represented in the figures. Following this model, the energy dissipated is a function of the slope angle and the speed of the avalanche at each position (Eq. A1). The DTM of the area, PCM model simulations and video images (event B) (Figure 6) were used to obtain these parameters.

Figures 8a and 8b show two estimations of the energy transmitted (Eq. 1) for event B using the speeds obtained through video images and PCM model simulations, respectively. As expected, the results are very similar. In both cases, an increase of the energy dissipated in the higher part of the path (between 100 and 400 m from the release zone) is observed. This increase is related to a big change of slope in the path profile. For larger distances the amplitude of the energy dissipated decreases considerably. The video images obtained reveal that the avalanche from approx. 600 m to 800 m had a deceleration and deposited part of its mass. This fact could be the explanation of the

decrease observed in the energy dissipated in that zone. We attribute the small discrepancies between the two different energy estimations (Figures 8a and 8b) to the misfit between the speed values predicted by the PCM and the video observations (Figure 6b). This misfit in speeds produce different estimations of the position of the avalanche front in the path at each instant of time (Sect. 3.3) and hence, in the avalanche front-seismometer distance (r), which is an input of Eq. 1. The increase in the estimated energy dissipated in the lower part of the path (distances >1200 m) mainly coincides with a decrease in the slope angle. As the slope angle decreases the dissipated energy increases; however, it never reaches the high values observed in the upper part of the path.

The energy per unit of mass obtained from the simple sliding block model simulation (Eq. A1) using video images and PCM model speed estimations are shown in Figures 8c and 8d, respectively. Although the comparison of the estimations of the energy transmitted (Eq.1, Figures 8a and 8b) with the results of the simulation is not straightforward because the evolution of the mass involved is not considered in the simulation, a good correlation among them is observed. In particular, the high amplitude zone corresponding with the change of slope at around 100 m predicted by the sliding block model is also observed in the energy transmitted into the ground. The very high amplitude zone observed from 200 to 400 is attributed to the body of the avalanche passing through the big change of the slope. The width of the peak obtained in the seismic estimations, which is not observed in the simulation, corresponds to the length of the avalanche. Taking into account that the model simulation considers the avalanche as a punctual sliding block, an estimation of the avalanche length in this part of the path of approximately 195 m could be given. A similar result was obtained through the energy estimation with the speeds from PCM. Although no detailed analysis of the

video images is available up to now our observations indicated that the event length is of this order. In the interval 500 m to 800 m the sliding block model predicts a relatively flat amplitude zone which is also observed in the seismic energy estimation (Figures 8 a and 8c). The peaks situated between approx. 800 and 1000 m are attributed to the big changes in the slope angle. The gradual increase observed in the estimated seismic energy dissipated for distances >1200 m (lower part of the path) (Figs 8a and 8b) is also predicted by the sliding block model (Figures 8c and 8d).

Figure 9 shows the results obtained for event A. Unfortunately, in this case only the PCM simulation (Figure 6a) was used because no direct speed measurements (e.g. video) in the upper part of the path existed. The estimations of the energy transmitted (Eq. 1) (Figure 9a) shows a similar shape than that of event B (Figure 8a). Two high amplitude peaks with similar order of magnitude and width as event B are observed in the upper part of the path and related to the change of slope. The sliding block model for this event predicts these two peaks (Figure 9b). In the 400-1200 m interval (Fig. 9a) the transmitted energy decreases to very low values. This is in contrast with that observed in event B, as well as, the result from the PCM simulations, where no energetic peaks are observed at this range. The high quantity of snow covering the area during the avalanche was probably the cause of this fact. The snow probably smoothed the topography of the path and diminished the contact of the base of the avalanche with the ground. The increase of the seismic energy for distances > 1000 m observed which is also predicted by the model is attributed to the decrease of the slope angle.

The evolutions of the seismic energy obtained for avalanches A and B seems to contradict the experience and also the sliding block model predictions. Owing to the incorporation of mass and the increase of the avalanche speed, as the avalanche evolves, we would expect the energy transmitted in the upper part to be smaller than that in the

lower part. However, when considering the source of the seismic signals generated by the avalanches an explanation to this apparent contradiction comes out. In earlier studies where seismic signals were compared with FMCW-radar measurements it was concluded that the main source of the seismic energy are the snow ploughing at the avalanche front and the erosion produced by the basal friction of the dense body inside the flow in contact with the ground (or snow cover) (Biescas et al., 2002). It is known that ploughing can be a dominant mechanism at the avalanche front when there is a rapid decrease in the slope angle in the direction of motion (McDougall and Hungr, 2005); In consequence, the high energetic peaks observed at approx. 200 m (Figure 8a, 8b) suggest that snow ploughing is the dominant mechanism for snow entrainment in the upper zone. Moreover, the low seismic energy values obtained by seismic methods for distances >400 m suggest that only a small part of the avalanche dense body generates seismic signals, probably only the snow in contact with the snow cover. The latter is supported by seismic observations of powder snow avalanches which generate very weak ground vibrations (Suriñach et al., 2001).

The total energy transmitted for avalanche B from the upper part of the path to UBtrack seismometer location is $4.2 \cdot 10^6$ J this value corresponds to a 0.03% of the potential energy of the avalanche if we consider that the mean mass of the avalanche was 18.900 T. This mass value was estimated as an average between the starting slab volume and the volume of the final deposits obtained in the corresponding subsequent field survey. Similar value of the total energy dissipated was obtained using the speeds from the PCM simulation ($4.1 \cdot 10^6$ J). The total energy transmitted for event A from the upper part of the path to the UBtrack seismometer location is $2.7 \cdot 10^6$ J. This value is slightly lower than that observed for event B. This result was expected due to the presence of

lower density snow in the dry/mixed avalanche (A) compared to the dry/dense avalanche (B).

5. Conclusions

A method to determine the seismic energy dissipated by snow avalanches and its evolution was developed and applied to two events of different type (dry/dense and dry/mixed artificially released avalanches). The seismic signals obtained from the explosions that triggered the avalanches recorded at two seismic stations were used besides the corresponding avalanche seismic signals. The energy determination needs a prior seismic characterization of the site and the knowledge of the avalanche front speed. In this paper a seismic characterization (surface waves phase velocity and attenuation factor) of the Ryggfonn site is presented. This characterization will serve for subsequent studies. The energy estimations obtained suggest that it is possible to identify the source of the seismic signals produced by the avalanche. The main source of seismic signals for the studied events corresponds to basal friction and ploughing at the avalanche front in changes of slope; the latter causing high seismic energy dissipation. The energies obtained could be a useful input parameter for the avalanche model validation and the presented method can be used as a new tool for empirical avalanche size classification.

The total energy dissipated from the top cornice to the location of the sensor in the avalanche path was obtained for the two events. The different type of these events, although they had the same size (4, Canadian size classification, McClung and Schaerer, 1993) is reflected in the seismic energy dissipated. The dry/mixed event dissipates a smaller amount of energy (2.7 MJ) than the dry/dense event (4.2 MJ).

This is supported by the comparison of the evolution of the seismic energy dissipated with the energy generated by a simple sliding block model of constant mass.

In the present study the speed of the avalanche front needed for the seismic energy estimation was obtained through video images and PCM model simulations owing to the data available. In this type of study, calibrated PCM model simulations proved to be useful in the case of lack of reliable avalanche front speeds. However, in cases of an adequate distribution of sensors, the seismic method presented in Vilajosana, et al, (2006) is a tool to precisely determine the speed of the avalanche front. This method and the method presented in this paper could be a good solution to estimate the seismic energy and became a good tool to determine the avalanche size from seismic measurements.

Appendix

Simple sliding block model

Simple sliding block models have been employed to calculate dipole-like basal force histories from the acceleration-deceleration phases of historical slides and to compare with the force histories inferred from seismic records (Kanamori, H., and J. W. Given., 1982, Brodsky et al., 2003). A theoretical estimation of the energy per unit of mass dissipated by the avalanche in a simple block model in the downslope direction is given by:

$$E_s(t) = -a_s(t) \cdot \Delta s(t) \quad (\text{Eq. A1})$$

Where Δs is the displacement experienced by the block in the down slope direction and

$$a_s(t) = g \cdot \sin \theta(t) - \mu \cdot g \cdot \cos \theta(t) - \xi \cdot v(t)^2 \quad (\text{Eq.A2})$$

is the down-slope component of the acceleration experienced by the sliding block; And g is the acceleration of gravity, θ is the slope angle, $v(t)$ is the speed of the avalanche front, ξ is drag friction coefficient and μ is the basal friction coefficient.

In our case the values of μ and ξ were chosen to be equivalent to the values used in the corresponding PCM simulations. Figures 8c, 8d and 9b show the energy per unit of mass dissipated into the ground by the sliding block using Eq. A1. The DTM (provided by NGI) was used to obtain θ . The speed values, v , were obtained from the PCM simulations and video images (event B).

Acknowledgements

The authors would like to thank to E. Lied and K. Kristensen for their support in Ryggfonn. This study is supported by the EU project SATSIE (EVG1-CT-2002-00059), MEC projects REN2002-12779-E/RIES and CGL2005-02250/BTE and the RISKMAT project of the Generalitat of Catalonia (PIGC: 2001SGR00081).

References

- Aki, K. and Richards, P.G., 1980. Quantitative Seismology. A series of books in geology, 1. W. H. Freeman and Company, New York, USA, 557 pp.
- Biescas, B., 2003. Aplicación de la sismología al estudio y detección de los aludes de nieve. Ph.D. Thesis, Universitat de Barceleona, Barcelona, Spain (ISBN: B. 46927-2003 / 84-688-3758-X), 1-130, <http://www.tdx.cesca.es/TDX-1010103-084042>.
- Biescas, B., Dufour, F., Furdada, G., Khazaradze, G. and Suriñach, E., 2003. Frequency content evolution of snow avalanche seismic signals. *Surveys in Geophysics*, 24: 447-464.
- Biescas, B., B. Sovilla, E. Suriñach, F. Tiefenbacher, F. Dufour, and G. Furdada, 2002. Correlation between seismic and radar FMCW signals of snow avalanches, *EGS XXVII General Assembly*, 4, Abstract EGS02-A-00879.

- Brodsky, E. E., Gordeev, E., and Kanamori, H., 2003. Landslide basal friction as measured by seismic waves, *Geophysical Research Letters*, 30, 2236.
- Firstov, P.P., Sukhanov, L.A., Pergament, V.Kh., y Rodionovskiy, M.V., 1992. Acoustic and seismic signal from snow avalanches. Transactions (Doklady) of the U.S.S.R. Academy of Sciences: Earth Science Sections, 312, 67-71, 1990. Scripta Technica, Inc., US. ISSN 0012-494X/90/0003, 12-15.
- Gauer, P., Kristensen, K. and Lied, K., 2004. Avalanche studies and model validation in Europe, SATSIE. Ryggfonn measurements Winter 2002/2003 and 2003/2004. 20021048-5, Norwegian Geotechnical Institute, Oslo (Norway).
- Gauer, P. and K. Kristensen. 2005. Ryggfonn measurements. Winter 2004/2005. NGI Report 20021048–8. Norges Geotekniske Institutt, Oslo, Norway.
- Jolly, A. D., Thompson, G., and Norton, G. E., 2002. Locating pyroclastic flows on Soufrière Hills volcano, Montserrat, West Indies, using amplitude signals from high dynamic range instruments, *Journal of Volcanology and Geothermal Research*, 118, 299-317
- Kanamori, H., and Given, J. W., 1982. Analysis of long-period seismic waves excited by the May 18, 1980, eruption of Mount St. Helens - a terrestrial monopole?, *Journal Geophysical Research*, 87, 5422–5432.
- Lied, K., Moe, A., Kristensen, K. and Issler, D., 2002. Ryggfonn: Snow Avalanche Research Programme SIP-6: Full scale avalanche test site and the effect of the catching dam, NGI report 581200-35, Norwegian Geotechnical Institute, Oslo, Norway.
- McClung, D. and Schaerer, P.A., 1993. *The Avalanche Handbook*, 98. The Mountaineers., 1011 SW Klickitat Way, Seattle, Washington, 134 pp.

- Nakamura, Y. 1989. A method for dynamic characteristics estimation of subsurface using microtremor on the ground surface. Quarterly Report of Railway Technical Research Institute (RTRI) 30:1, 25-33.
- Perla, R., Cheng, T. T. and McClung, D. M., 1980. A two-parameter model of snow-avalanche motion. Journal of Glaciology Vol 26, No. 94 pp. 197--207.
- Suriñach, E., Sabot, F., Furdada, G. and Vilaplana, J.M., 2000. Study of seismic signals of artificially released snow avalanches for monitoring purposes. Physics and Chemistry of the Earth, 25(9): 721-727.
- Suriñach, E., Furdada, G., Sabot, F., Biescas, B. and Vilaplana, J.M., 2001. On the characterization of seismic signals generated by snow avalanches for monitoring purposes. Annals of Glaciology, 32: 268-274.
- Suriñach, E., 2004. Spanish avalanche research: Experimental sites and seismic measurements. En: Naaim M, Naaim-Bouvet (ed.) 2004. Snow and Avalanche Test Sites, Cemagref, 71-183.
- Suriñach, E., I. Vilajosana, G. Khazaradze, B. Biescas, G. Furdada, and J. M. Vilaplana. 2005. Seismic detection and characterization of landslides and other mass movements. Natural Hazards and Earth System Sciences 5, 791–798; SRef-ID: 1684–9981/nhess/2005–5–791.
- Suwa, H., Akamatsu, J. and Nagai, Y., 2003. Energy radiation by elastic waves from debris flows. Debris flows hazard mitigation: mechanics, prediction and assesement. Millpress, Rotterdam.
- Tatom, F.B. and Vitton, S.J., 2001. The Transfer of Energy from a Tornado into the ground. Seismological Research Letters, 72(1): 12-21.

Vilajosana, I., G. Khazaradze, E. Suriñach, E. Lied and K. Kristensen. 2006. Snow avalanches speed determination using seismic methods. Submitted to Cold Regions Sci. and Technol. (EGU 2005 special issue).

Figure captions

Figure 1. Detailed profile of the lowest part of the avalanche path at Ryggfonn including the installed instrumentation. The Inset in the upper right corner shows the complete Ryggfonn avalanche path profile. Geophones (GF), load plates (Lp), load cells (Lc). The origin of the distances is set to the location of the explosion that triggers the avalanches.

Figure 2. Map of the Ryggfonn area. Star: position of the explosion that triggered the avalanches. Dots: position of the University of Barcelona seismometers. Location of the Dam is also indicated. UTM coordinates are used.(Source NGI).

Figure 3. Propagation model for surface waves. r distance avalanche front-seismometer; v avalanche speed; h $\frac{1}{4}$ of the wave length.

Figure 4. Ryggfonn Q amplitude attenuation factor in function of the frequency. Line: linear fitting: $Q = 0.087 \cdot f + 5.3$.

Figure 5. Avalanche ground motion (mm/s) seismograms for event A (left) and event B (right). From top to bottom: Vertical, North, East components of the seismic signals registered in UBTrack. Origin of time set to the explosion that triggered the avalanches.

Figure 6. Left: Avalanche front speed from PCM models simulation for event A (continuous line). Right: Front speed estimations from video (dotted line) and avalanche front speed from PCM models simulation (continuous line) for event B. The path profile is represented as a dashed line in the background of the plots. Origin of distances set to the explosion location.

Figure 7. Ground motion velocity representation for event B. Top: Z, N, E components of the seismic signal between 10 and 11 s. Bottom: ground motion velocity in the vertical plane (Z-N and Z-E) and in the horizontal plane (N-E).

Figure 8. Energy dissipated by surface waves (horizontal components) for event B using speed obtained from video (a) and speed obtained from PCM simulation (b). Energy per unit of mass obtained from the sliding block simulation using speed from Video images (c) and speed from PCM (d). The path profile is depicted in the background of these plots as a continuous line. The origin of distances is set to the location of the explosions.

Figure 9. a) Energy dissipated by surface waves (horizontal components) for event A using speed obtained from PCM simulation. b) Energy per unit of mass obtained from the sliding block simulation using speed from PCM. The path profile is depicted in the background of these plots as a continuous line. The origin of distances is set to the location of the explosions.

Figure1

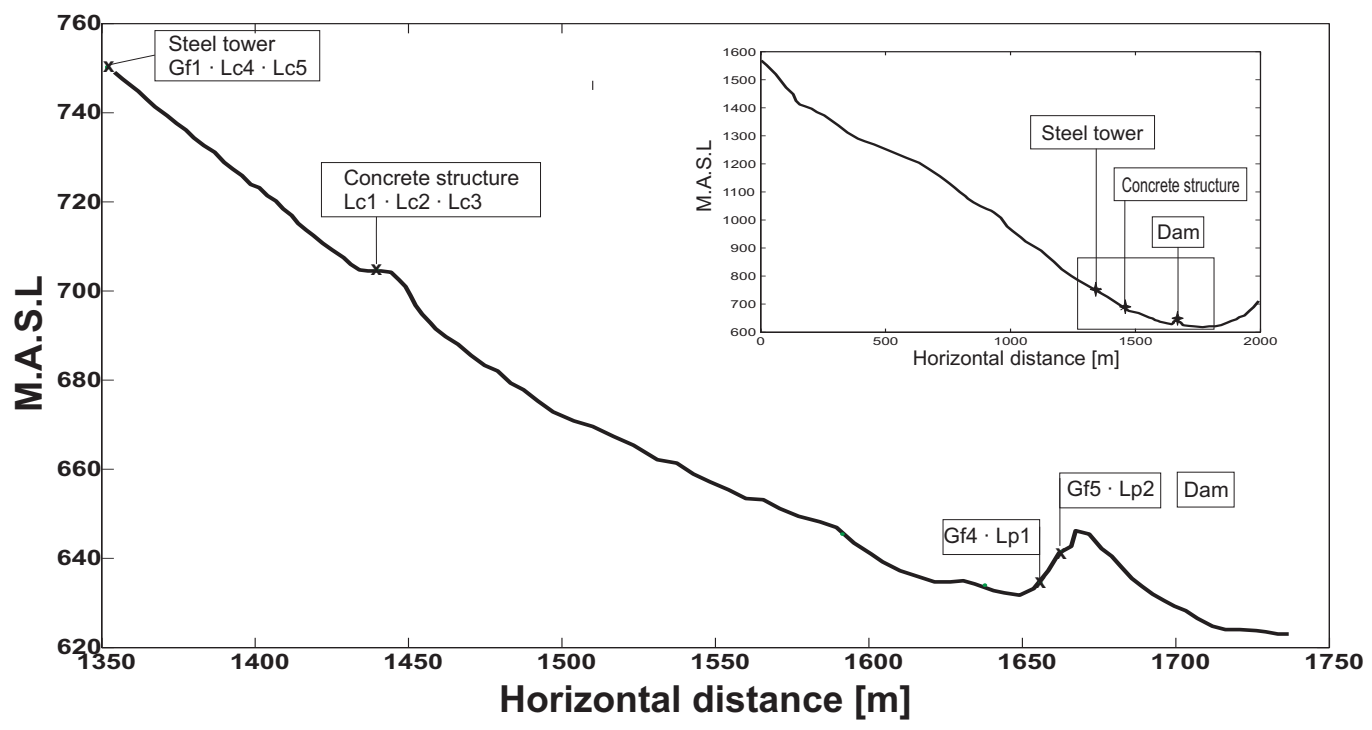


figure2

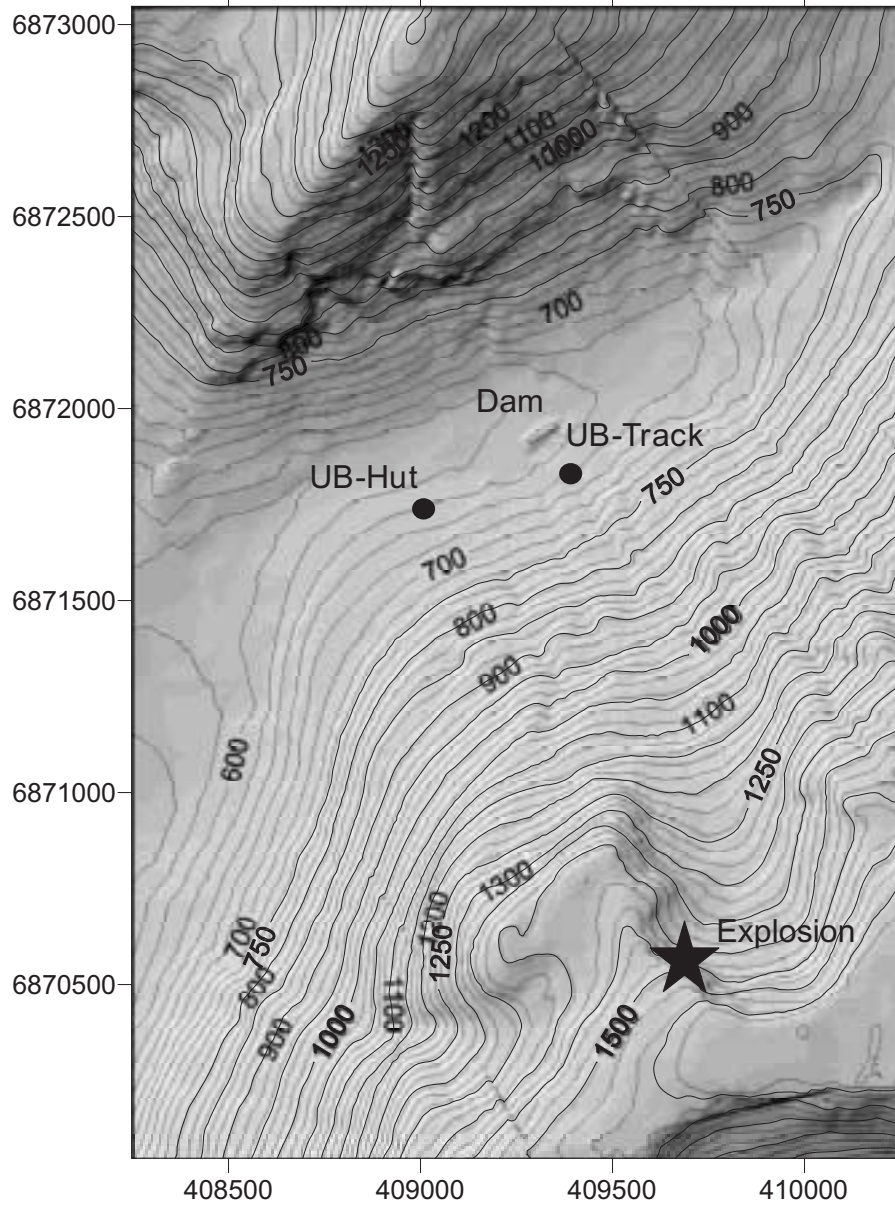


Figure3

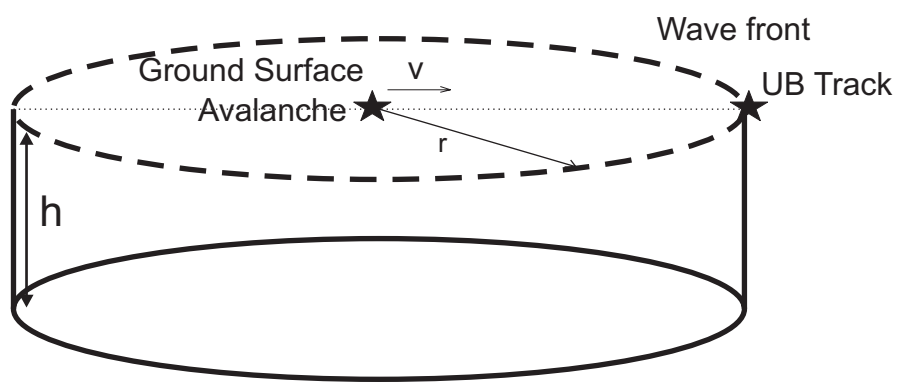


Figure4

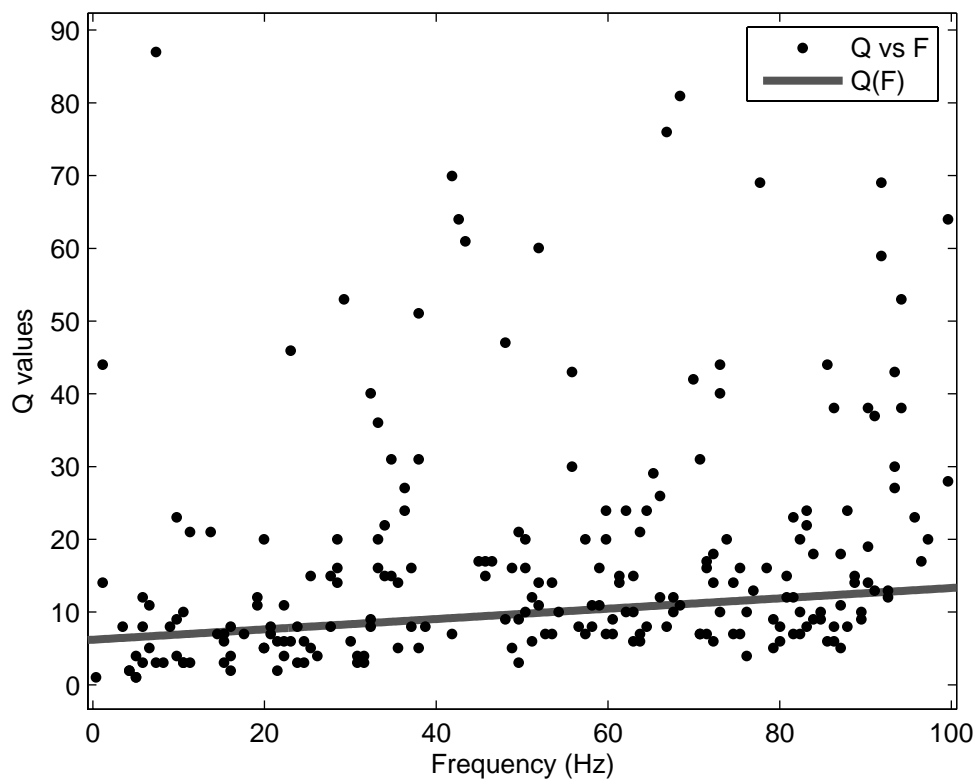


Figure5

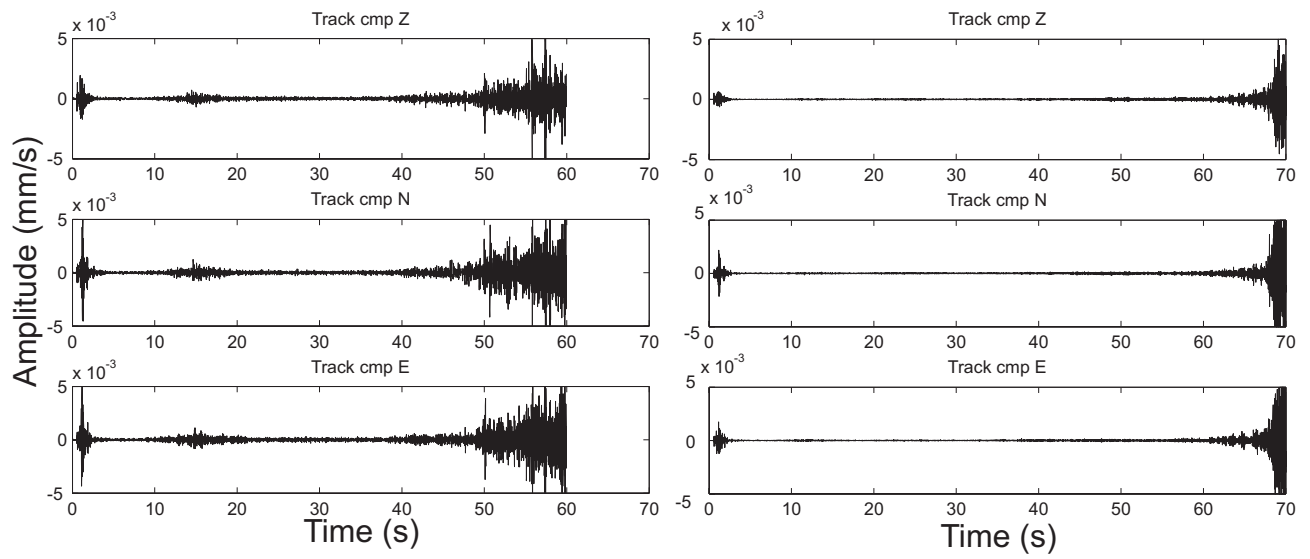


Figure6

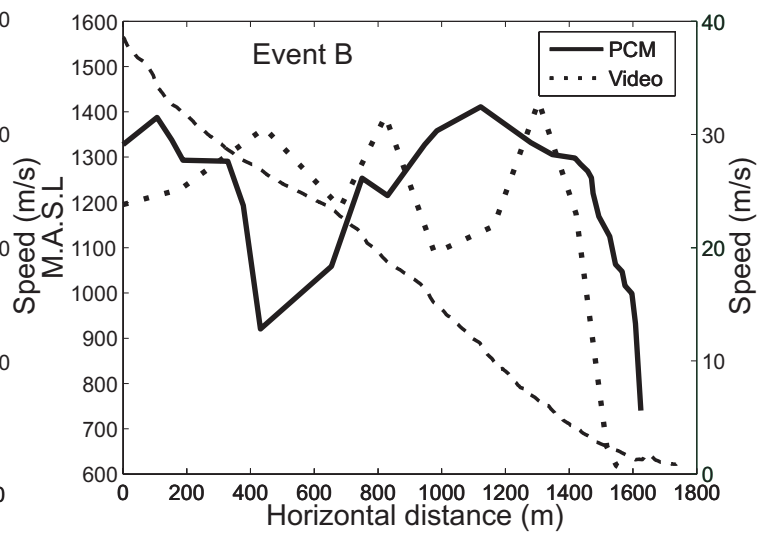
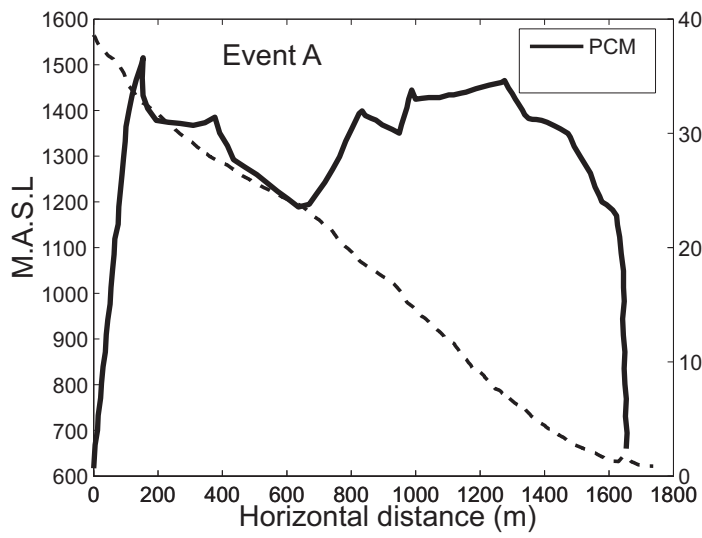


Figure7

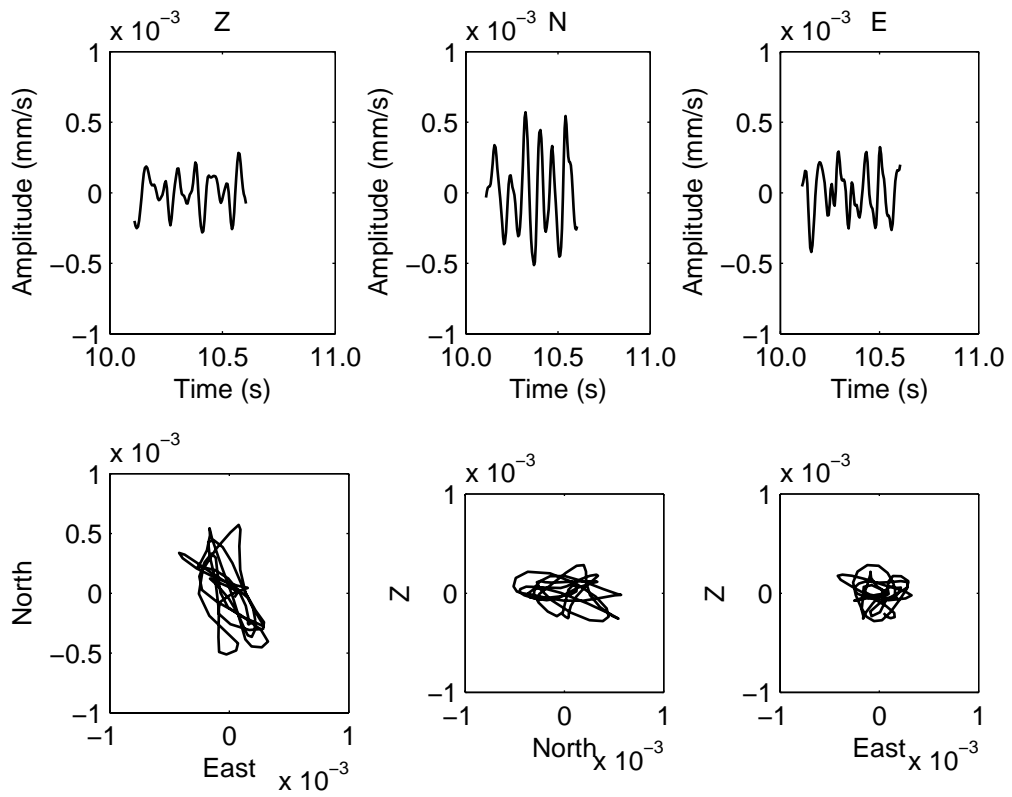


Figure8

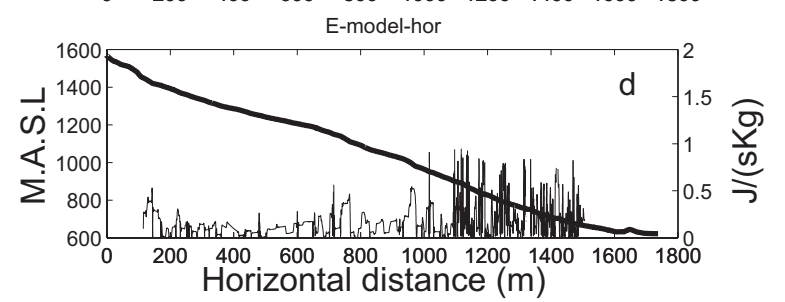
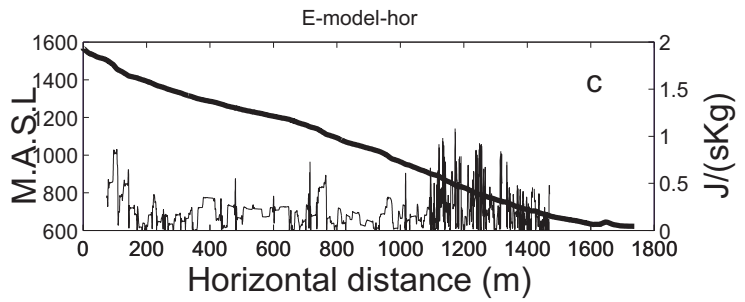
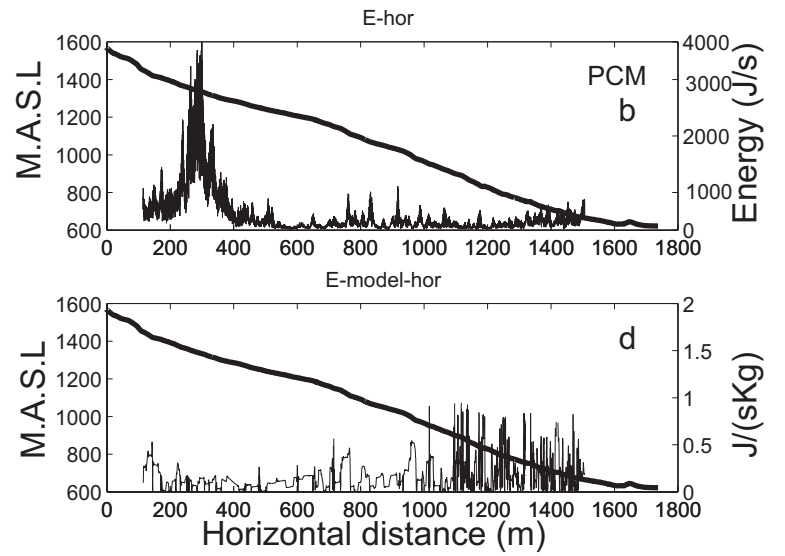
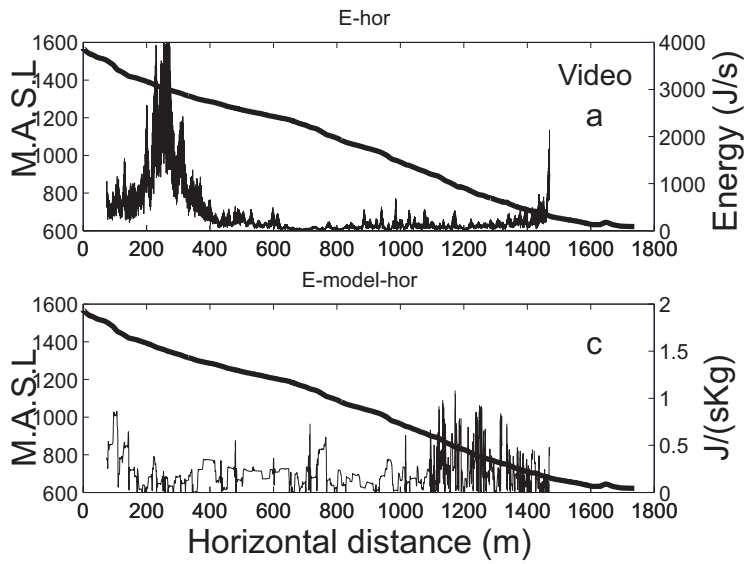


Figure9

